Physics in Medicine & Biology

PAPER

Medical image registration by combining global and local information: a chain-type diffeomorphic demons algorithm

To cite this article: Xiaozheng Liu *et al* 2013 *Phys. Med. Biol.* **58** 8359

IOP Publishing Physics in Medicine and Biology

Phys. Med. Biol. **58** (2013) 8359–8378 doi:10.1088/0031-9155/58/23/8359

Medical image registration by combining global and local information: a chain-type diffeomorphic demons algorithm

Xiaozheng Liu[1], **Zhenming Yuan**[2], **Junming Zhu**[3] **and Dongrong Xu**[4,5]

[1] Zhejiang Key Laboratory for Research in Assessment of Cognitive Impairments, Center for Cognitive Brain Disorders, Hangzhou Normal University, Hangzhou 310015, People's Republic of China
[2] Department of Information Science and Engineering, Hangzhou Normal University, Hangzhou 310012, People's Republic of China
[3] Department of Neurosurgery, The Second Affiliated Hospital of Zhejiang University, Hangzhou 310009, People's Republic of China
[4] MRI Unit, Department of Psychiatry, New York State Psychiatric Institute, Columbia University, NYSPI Unit 74, 1051 Riverside Drive, New York, NY 10032, USA

E-mail: dx2103@columbia.edu

Received 1 May 2013, in final form 2 September 2013
Published 11 November 2013
Online at stacks.iop.org/PMB/58/8359

Abstract

The demons algorithm is a popular algorithm for non-rigid image registration because of its computational efficiency and simple implementation. The deformation forces of the classic demons algorithm were derived from image gradients by considering the deformation to decrease the intensity dissimilarity between images. However, the methods using the difference of image intensity for medical image registration are easily affected by image artifacts, such as image noise, non-uniform imaging and partial volume effects. The gradient magnitude image is constructed from the local information of an image, so the difference in a gradient magnitude image can be regarded as more reliable and robust for these artifacts. Then, registering medical images by considering the differences in both image intensity and gradient magnitude is a straightforward selection. In this paper, based on a diffeomorphic demons algorithm, we propose a chain-type diffeomorphic demons algorithm by combining the differences in both image intensity and gradient magnitude for medical image registration. Previous work had shown that the classic demons algorithm can be considered as an approximation of a second order gradient descent on the sum of the squared intensity differences. By optimizing the new dissimilarity criteria, we also present a set of new demons forces which were derived from the gradients of the image and gradient magnitude image. We show that, in controlled experiments, this advantage is confirmed, and yields a fast convergence.

(Some figures may appear in colour only in the online journal)

[5] Author to whom any correspondence should be addressed.

1 Introduction

During the past 20 years, many techniques have been developed for non-rigid registration (Holden 2008, Hawkes 1999, Thirion 1998). Most of them build a parameterized model that constrains the form of allowed deformations, and then optimizes a variational energy function with the aim of minimizing the dissimilarity between images. In this paper, we focus on assessing and improving a deformable registration algorithm that was proposed by Thirion (1998). This algorithm, also called the 'demons' algorithm, performs registration between a fixed image (the target image), and its deformed moving image (the source image). The algorithm iteratively minimizes the measure of difference between image intensities. The driving force corresponds to the gradient of image intensity of the fixed image (Thirion 1998). However, the classic demons algorithm, using image gradient information from the dissimilarity of image intensity, is highly sensitive to local artifacts and easily trapped in a local minimum.

Many variants of the demons forces have been proposed to improve the demons-type algorithm (Pennec *et al* 1999, Vercauteren *et al* 2008, 2009, Cachier *et al* 2003, Rogel and Kovacic 2006, Wang *et al* 2005, Cheng and Mrinal 2010, Luo and Chung 2009, Gu *et al* 2010, Nathan *et al* 2009, Hernandez and Olmos 2008). Considering that the registration may be made more efficient when the deformation is bi-directional, several variants of symmetric demons (SymD) forces that include gradient information of both the moving image and the fixed image have been defined (Rogel and Kovacic 2006, Wang *et al* 2005). Because the demons algorithm moves pixels along gradient direction, information orthogonal to the direction of the gradient is lost. Cheng and Mrinal (2010) used a symmetric orthogonal gradient to calculate the demons forces and showed that the registration was more accurate. Luo and Chung (2009) introduced a new feature-based image, a local histogram of the intensity image, to substitute the original intensity image. Their method utilized geometric moments of local histograms to form new feature images. The local histogram-based features are rotation invariant and can capture sufficient spatial information of an image. Meanwhile, mutual information had been embedded into the demons framework for the purpose of multimodal registration (Kroon and Slump 2009, Modat *et al* 2010). However, most demons-type algorithms just used an additive adjustment rule to update a deformation field that was not smooth and invertible, so the deformation process of these algorithms was not diffeomorphic (Arsigny *et al* 2006, Ashburner 2007, Beg *et al* 2005, Avants *et al* 2006, Rueckert *et al* 2006).

Vercauteren *et al* (2009) developed a diffeomorphic demons (DD) algorithm by using an intrinsic update rule on the Lie group through an exponential map. They also gave a unified theoretical justification for the demons algorithm and showed that different image registration frameworks can be used for image registration and the different variants are related to the use of different optimizers. However, Vercauteren *et al* (2009) used differences between image intensities to get the demons forces. While, medical images are vulnerable to a number of artifacts, including noise and non-uniformities, so similarities based on differences in image intensity is easily affected by such imaging artifacts.

Compared with intensity information which is the global information of an image, the gradient magnitude that is extracted from the local information of an image has the following properties: (1) the difference in gradient magnitude obtained from local information of an image is more robust than the simple difference between image intensities for local artifacts (figure 1); (2) the gradient magnitude image represents structural information of an image, while the aim of registration is to align the structure of different tissue types. Therefore, we assume that the dissimilarity including the difference in gradient magnitude has a good effect on the structural alignment in medical image registration.

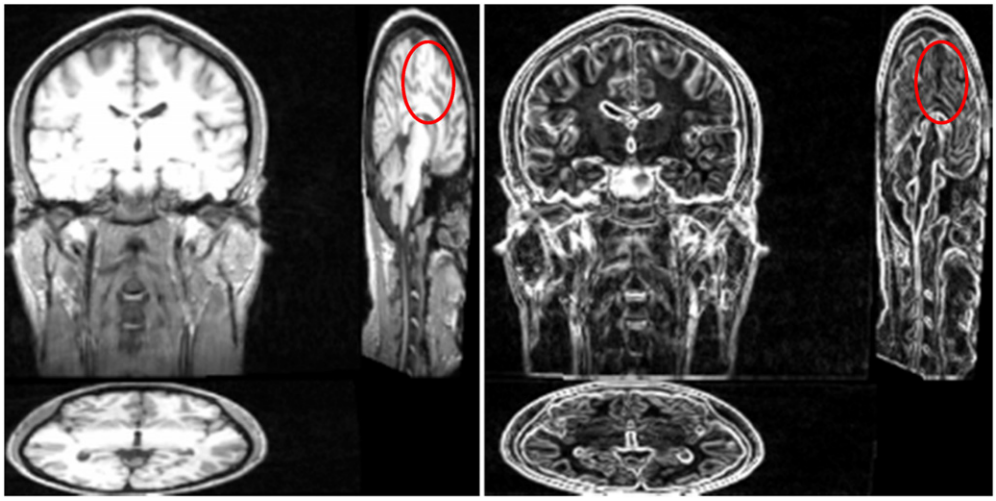

Figure 1. Intensity image and gradient magnitude image of a T1 MRI image. (a) Example slices of a T1-weighted image. (b) Gradient magnitude images corresponding to (a). The gradient magnitude image reflects the structure information of an image. The red circle in (a) indicates a non-uniform region where the voxel intensity values are statistically higher than in all other regions in the brain, however this non-uniformity is eliminated in the corresponding gradient magnitude image (red circle in (b)). (Images provided by the Center for Morphometric Analysis at Massachusetts General Hospital and are freely available at (http://www.cma.mgh.harvard.edu/ibsr/data.html).

Based on the above consideration, we propose a demons-type registration algorithm that considers both the differences in the image intensity and gradient magnitude for medical image registration. Although gradient information had been used in other types of registration methods (Rui *et al* 2008, Roger *et al* 2003), to the best of our knowledge, the combination of the differences of both image intensity and gradient magnitude has not been used in demons-type algorithms. Because it has been demonstrated that the demons algorithm is equivalent to a Levenberg–Marquardt optimization of the mean squared difference (MSD) between the images to register (Pennec *et al* 1999), the MSD, including the differences between both image intensities and gradient magnitudes, can be assumed for optimization and registration. In addition, our method is the first registration method which not only uses both global and local information of an image but also can remain diffeomorphic.

This paper is organized as follows. In section 2, we first review the DD algorithm with a unified framework for mono-modal image registration. Then we introduce our new method, a chain-type DD algorithm, which combines the differences of both image intensity and gradient magnitude into the demons algorithm. Like the works in Vercauteren *et al* (2009), a new set of demons forces corresponding to different optimization methods are also given for the new method. Experiments are presented in section 3. Finally, section 4 concludes the paper with detailed discussions on a number of issues.

2 Methods

2.1. Diffeomorphic demons

Given two images, a fixed image F and a moving image M, non-parametric image registration aims to find a transformation s: $p \rightarrow s(p)$ to get a accurate alignment of the images. The transformation s models the spatial mapping of points from the fixed image space to the

moving image space. In general, the registration problem can be formulated as an optimization problem that minimizes a dissimilarity measure Dis(·) between images. The classic demons algorithm can be regarded as the following energy function:

$$E(s) = \frac{1}{\sigma_i^2}\mathrm{Dis}(F, M, s) + \frac{1}{\sigma_T^2}\mathrm{Re}\ g(s) \tag{1}$$

where σ_i weighs the intensity uncertainty of the images, and σ_T weighs the transformation uncertainty of s alone. The dissimilarity criterion Dis(·) illustrates the resemblance between two images, usually representing the mean squared error (MSE), and Re $g(s)$ is a regularization term. However, two steps are needed to minimize the above energy function, which make it not a global energy function (Vercauteren *et al* 2009).

In order to cast the demons algorithm into the optimization of a well-posed criterion, a hidden variable c was introduced in the registration process to construct a global energy function:

$$E_g(c, s) = \frac{1}{\sigma_i^2}\mathrm{Dis}(F, M, c) + \frac{1}{\sigma_x^2}\mathrm{dist}(s, c)^2 + \frac{1}{\sigma_T^2}\mathrm{Re}\ g(s) \tag{2}$$

where σ_x weighs the spatial uncertainty between c and s. The term $\mathrm{dist}(s, c)^2$ imposed on the displacement field s ensures that s is close to the correspondence field c.

The introduction of the hidden variable c allows the energy to be split into two forms, each of which can be optimized alternately in the following scheme (Cachier *et al* 2003).

(1) Correspondence: given the current s, find c by minimizing

$$\frac{1}{\sigma_i^2}\|F - M \circ c\|^2 + \frac{1}{\sigma_x^2}\mathrm{dist}(s, c)^2. \tag{3}$$

(2) Regularization: find s by minimizing

$$\frac{1}{\sigma_x^2}\mathrm{dist}(s, c)^2 + \frac{1}{\sigma_T^2}\mathrm{Re}\ g(s). \tag{4}$$

In general, the first step finds the optimization correspondence field c by minimizing equation (3). The second step is the convolution of the correspondence field by a Gaussian kernel if the regularization is quadratic and uniform (Vercauteren *et al* 2009).

However, the classic demons algorithm used an additive rule to update the deformation field by $c = s + u$, if small deformations are parameterized by a dense displacement field u. For s to be a meaningful transformation in biomedical image registration, an intrinsic update rule on the Lie group through the exponential map, $c = s \circ \exp(u)$, has been proposed to ensure the diffeomorphic property of the resulting transformation (Vercauteren *et al* 2009, Kroon and Slump 2009).

After embedding the new update rule into the global energy function E_g and defining the criteria of the dissimilarity, distance and regularization for the global energy in equation (2) as $\mathrm{Dis}(F, M, c) = ||F - M \circ c||^2$, $\mathrm{dist}(s, c) = ||Id - s^{-1} \circ c||$ and Re $g(s) = ||\nabla s||^2$, we can optimize the global energy function in equation (2) alternatively in the following scheme (Vercauteren *et al* 2009).

2.2. Chain-type diffeomorphic demons

In this section, we will introduce a new dissimilarity measure that combines the differences of both image intensity and gradient magnitude for the demons algorithm and propose a new set of demon forces that includes the gradient of both image intensity and gradient magnitude.

Algorithm 1 (DD).

- Choose a starting spatial transformation s (represented by a displacement field).
- Iterate until convergence.
- Given s, compute a correspondence update field u by minimizing the first two terms of equation (2): $u = \arg\min_{u} \|F - M \circ s \circ \exp(u)\|^2 + \frac{\sigma_i^2}{\sigma_x^2}\|u\|^2$ with respect to u.
- If a fluid-like regularization is used, let $u \leftarrow K_{\text{fluid}} * u$. The convolution kernel will typically be a Gaussian kernel.
- Let $c \leftarrow s \circ \exp(u)$.
- If a diffusion-like regularization is used, let $s \leftarrow K_{\text{diff}} * c$ (else let $s \leftarrow c$). The convolution kernel is also typically Gaussian.

Initially, a new dissimilarity criterion that measures the differences of both image intensity and gradient magnitude can be defined as follows:

$$\text{Dis}(F, M \circ c, \|\nabla F\|, \|\nabla(M \circ c)\|) = \frac{1}{2}\|F - M \circ c\|^2 + \frac{\alpha}{2}\|\|\nabla F\| - \|\nabla(M \circ c)\|\|^2 \tag{5}$$

where α is a weighting factor. $\|\nabla F\|$ is the gradient magnitude of the fixed image and $\|\nabla(M \circ c)\|$ is the gradient magnitude of the moving image. We construct a new global energy function using the above dissimilarity criterion (Vercauteren *et al* 2009):

$$E_g(c, s) = \frac{1}{\sigma_j^2}\text{Dis}(F, M, \|\nabla F\|, \|\nabla(M \circ c\|) + \frac{1}{\sigma_y^2}\text{dist}(s, c)^2 + \frac{1}{\sigma_T^2}\text{Re } g(s) \tag{6}$$

where σ_y and σ_j are similar to σ_x and σ_i in equation (2), but are all constrained by the differences in both image intensity and gradient magnitude. We chose the same distance function (Vercauteren *et al* 2009), regularization function and update form, $\text{dist}(s, c) = ||Id - s^{-1} \circ c||$, $\text{Re } g(s) = ||\nabla s||^2$ and $c = s \circ \exp(u)$, for the new energy function (equation (6)).

The only difference between our method and the DD algorithm lies in the first step of algorithm 1. The DD algorithm minimizes equation (3) to find the update field u, while our method minimizes the following function to find the update field u:

$$E_{\text{cd}} = \frac{1}{2}\|F - M \circ s \circ \exp(u)\|^2 + \frac{\alpha}{2}\|\|\nabla F\| - \|\nabla(M \circ s \circ \exp(u)\|\|^2 + \frac{\sigma_j^2}{\sigma_y^2}\|u\|^2. \tag{7}$$

In order to establish an analytical expression for the deformation field u, we can consider the intensity difference at a given point $\varphi_p(s) = F(p)\text{-}M \circ s(p)$. After letting $\varphi^s{}_p(u) = F(p)\text{-}M \circ s \circ \exp(u)(p)$ in the diffeomorphic case, we can assume that the following linearization is available (Vercauteren *et al* 2009):

$$\varphi_p^s(u) \approx \varphi_p^s(0) + J^p \cdot u(p) \tag{8}$$

where J^p is the corresponding Jacobian matrix (Vercauteren *et al* 2009). Then, we can consider a first order expansion of the differences in image intensity and the differences in gradient magnitude, respectively:

$$F(p) - M \circ s \circ \exp(u)(p) \approx F(p) - M \circ s(p) + J^p \cdot u(p) \tag{9}$$

$$\|\nabla F(p)\| - \|\nabla(M \circ s \circ \exp(u)(p))\| \approx \|\nabla F(p)\| - \|\nabla(M \circ s(p))\| + J_{\text{g}}^p \cdot u(p) \tag{10}$$

where J^p and $J_g{}^p$ are Jacobian matrices of the intensity image and the gradient magnitude image, respectively. By using these two expansions, we get the following expression for the approximation of the correspondence energy:

$$E_{\text{cd}}(u) = \|F - M \circ s(p) + J^p \cdot u(p)\|^2 + \alpha \left\|\|\nabla F\| - \|\nabla(M \circ s(p)\| + J_g^p \cdot u(p)\right\|^2 + \frac{\sigma_j^2}{\sigma_y^2}\|u\|^2. \tag{11}$$

Table 1. Demons variants according to the different demons forces.

Image intensity, J^p	Gradient magnitude image, J_g^p	Variance
$J^p = -\nabla_p^T(M \circ s)$	$J_g^p = -\nabla_p^T(\|\nabla(M \circ s)\|)$	Thirion mov
$J^p = -\nabla_p^T(F)$	$J_g^p = -\nabla_p^T(\|\nabla F\|)$	Thirion fix
$J^p = -(\nabla_p^T F + \nabla_p^T M \circ s)/2$	$J_g^p = -(\nabla_p^T\|\nabla F\| + \nabla_p^T(\|\nabla(M \circ s)\|)/2$	Thirion sym
$J^p = -\nabla_{s(p)}^T M$	$J_g^p = -\nabla_{s(p)}^T\|\nabla M\|$	Pennec (99)

In this table, Thirion refers to the variants proposed in (Thirion 1998), and Pennec 99 refers to the variant proposed in (Pennec *et al* 1999).

Then, we can calculate the error gradient of the energy function E_{cd} as

$$\nabla E_{\text{cd}}(u) = 2(J^p)^T(F - M \circ s(p) + J^p \cdot u(p)) + 2(J_g^p)^T\alpha(\|\nabla F\| - \|\nabla(M \circ s(p)\| + J_g^p \cdot u(p)) + 2\frac{\sigma_i^2}{\sigma_y^2}u. \tag{12}$$

Assuming that ∇E_{cd} is minimum at $\nabla E_{\text{cd}}(u) = 0$, we can calculate the needed update:

$$u(p) = \frac{-(F(p) - M \circ s(p))J^{p^T} - \alpha(\|\nabla F(p)\| - \|\nabla M \circ s(p)\|)(J_g^p)^T}{\|J^p\|^2 + \left\|J_g^p\right\|^2 + \frac{\sigma_i^2}{\sigma_y^2}} \tag{13}$$

where $\frac{\sigma_i^2(p)}{\sigma_y^2}$ is basically a regularization parameter that should be adaptively set according to specific conditions. According to the DD algorithm, we split this regularization parameter into two terms:

$$\frac{\sigma_i^2(p)}{\sigma_y^2} = \frac{\sigma_{i1}^2(p)}{\sigma_y^2} + \frac{\sigma_{i2}^2(p)}{\sigma_y^2} \tag{14}$$

where $\frac{\sigma_{i1}^2(p)}{\sigma_y^2}$ accounts for the image noise and $\frac{\sigma_{i2}^2(p)}{\sigma_y^2}$ accounts for the noise of the gradient magnitude image. If we use the local estimation of the image noise, $\sigma_{i1} = \|F(p) - M \circ s(p)\|$, and the local estimation of the noise of the gradient magnitude images, $\sigma_{i2} = \|\|\nabla F(p)\| - \|\nabla M \circ s(p)\|\|$, we end up exactly with a new expression of the demons forces of our method. Then, equation (13) becomes:

$$u(p) = \frac{-(F(p) - M \circ s(p))J^{p^T} - \alpha(\|\nabla F(p)\| - \|\nabla M \circ s(p)\|)(J_g^p)^T}{\|J^p\|^2 + \frac{\sigma_{i1}^2(p)}{\sigma_y^2} + \left\|J_g^p\right\|^2 + \frac{\sigma_{i2}^2(p)}{\sigma_y^2}}. \tag{15}$$

From equation (15), it can be seen that our method unifies different image information into one deformation field by a chain-type formula, so we name our method a chain-type DD algorithm.

Like that in (Vercauteren *et al* 2009), the linearization of the differences in image intensity and gradient magnitude is needed to put in the expression of the demons forces in equation (15). In (Vercauteren *et al* 2009), the authors showed that the unified framework they used to explain the different demons forces could be used in the DD with different types of optimizers. Because the gradient magnitude image is also a digital image and carries only gradient information, the linearization of the difference in gradient magnitude is similar to that of the intensity. The complete set of variants of the demons is summarized in table 1.

3. Experiment

We implemented the registration methods within the Matlab R2010a environment using a personal computer configured with a 3.40 GHz Quad Core Intel i7–2600 CPU and 8 GB of

RAM running 64-bit Windows 7. We compared our method with the DD algorithm using the popularly used versions of the demons forces, including the fixed image force, the moving image force and the symmetric image force, which in the literature have never been carefully evaluated within a registration procedure of 3D MRI images in previous works. We also compared our method with another popular SymD algorithm proposed by Wang *et al* (2005).

We performed three sets of experiments to assess the effectiveness of our proposed model for MRI images registration. In the first and second experiments, we used simulated datasets to demonstrate the theoretical soundness of our model. In the third experiment, we used real MRI image datasets of human brains to examine the performance of our model in practice. We employed the simulated datasets because we would like to minimize potential disturbance from those uncontrolled variables (e.g., image distortion, mismatches between corresponding voxels, etc) that is hard to be excluded in using real world data, so that the effectiveness of our method can be clearly evaluated. We used real data for verifying that our method can work properly and efficiently in practice.

In the first experiment, we aimed to examine and compare the resistance ability of the three methods to noise and intensity non-uniformities, in which we used simulated MRI data with different levels of noise and intensity non-uniformities. We downloaded three T2-weighted images from the McGill Brain Web[6], each containing three different noise levels (0%, 5%, 9%) and three different intensity non-uniformity levels (0%, 20%, 40%).

In the second experiment, 20 simulated T1 MRI image volumes from different subjects were downloaded from BrainWeb (see footnote 6). The size of each image volume was $256 \times 256 \times 181$ pixels. All voxels had already been segmented and labeled with one of the three tissue classes, which are white matter (WM), gray matter (GM), and cerebrospinal fluid (CSF).

In the third experiment, a set of real 18 T1 MRI images from the Internet Brain Segmentation Repository (IBSR) was employed to compare performance of the registration algorithms. Image size was $256 \times 256 \times 128$ pixels with a voxel size of $0.94 \times 0.94 \times 1.5$ mm^3. The 18 selected image volumes were manually segmented into three classes of tissues: WM, GM and CSF as provided by the IBSR website. The images and their manual segmentations were provided by the Center for Morphometric Analysis at Massachusetts General Hospital and are freely available at (http://www.cma.mgh.harvard.edu/ibsr/data.html).

3.1. Experiment design

To analyze precisely the registration accuracy of the proposed method, the following three criteria were used to quantify the quality of alignment in the image coordinates: (1) the relative sum of squared differences (RSSD) between the fixed images and the deformed image was used to quantify the image match (Hernandez *et al* 2008),

$$\mathrm{RSSD} = \sqrt{\frac{\sum_{i=1}^{N} (F - M \circ c)^2}{\sum_{i=1}^{N} (F - M)^2}} \tag{16}$$

where F is the fixed image, M is the moving image, $M \circ c$ is the deformed moving image, and N is the total number of voxels in the image. The RSSD provides a good trade-off between intensity match and degree of deformation. The lower values of RSSD indicate better alignment. (2) The normalized cross-correlation (NCC) (Kai and Uwe 2001, Sabuncu *et al* 2009) is based on the assumption that there is a linear relationship (up to some noise) between

[6] www.bic.mni.mcgill.ca/brainweb/.

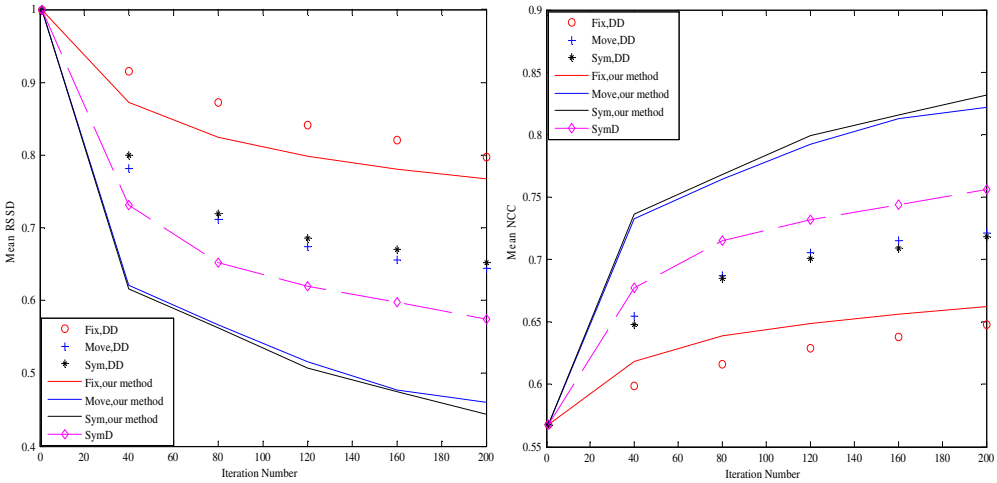

(a) (b)

Figure 2. Performance comparisons of simulated T2-MRI images by DD, SymD and our method using (a) mean RSSD and (b) mean NCC.

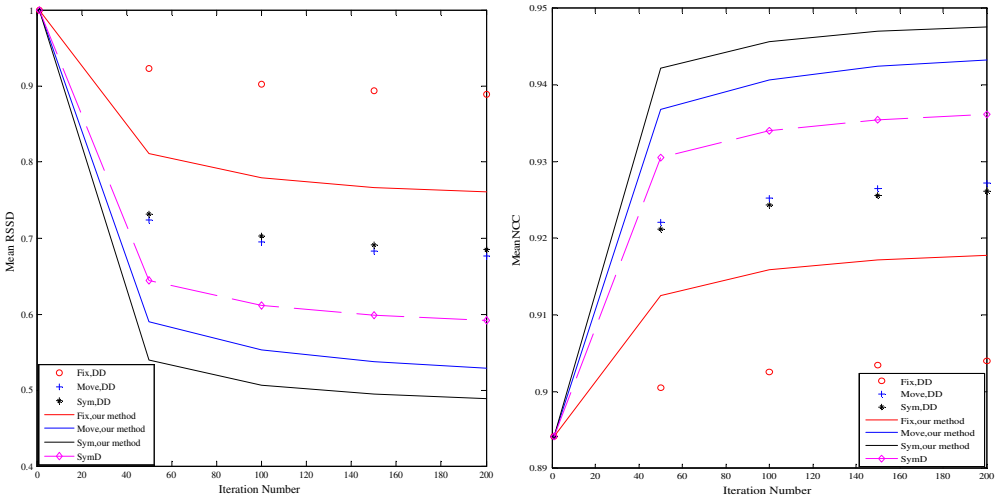

(a) (b)

Figure 3. Performance comparisons of simulated T1-MRI images by DD, SymD and our method using (a) mean RSSD and (b) mean NCC.

corresponding voxel intensity values. NCC is related to the well-known Pearson's correlation between corresponding intensity values of the two images:

$$\mathrm{NCC} = \sum_{i,j,k} \frac{(F(i,j,k) - \overline{F})((M \circ c)(i,j,k) - \overline{M \circ c})}{\sigma_F \sigma_M} \tag{17}$$

where $\overline{F}$ and $\overline{M \circ c}$ are the mean values of the fixed and deformed image at each voxel, respectively; σ_F and σ_M are the voxel-wise variances of the fixed image and deforming image, respectively. The NCC is invariant to linear brightness and contrast variations, so NCC is more robust than MSE (Hernandez *et al* 2008) with respect to registration accuracy. NCC varies

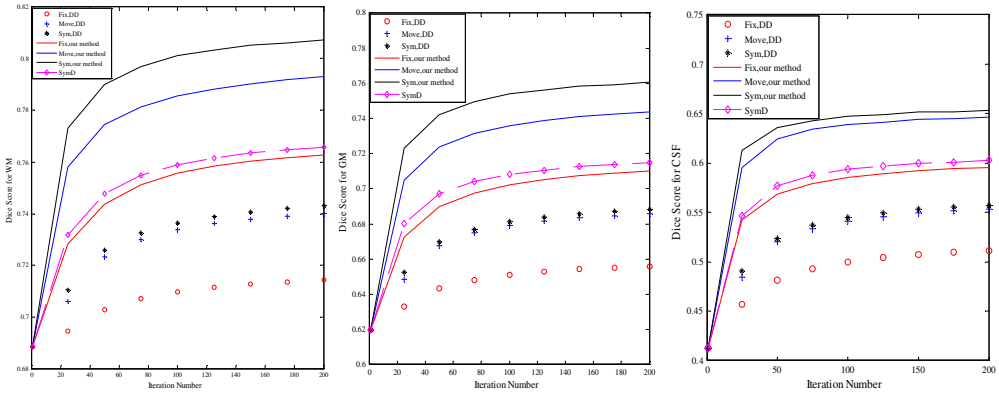

(a) (b) (c)

Figure 4. Comparisons of Dice Scores for the three tissue types of the simulated T1-MRI images: WM, GM and CSF. (a) Dice score for white matter, (b) Dice score for gray matter and (c) Dice score for CSF.

Table 2. Comparisons of the normalized cross correlation obtained from the registration of the simulated T1-weighted MR images. The column is number of the sample data. The row is the results of different methods. The best results are shown in bold.

	Fix, DD	Move, DD	Sym, DD	Fix, our method	Move, our method	Sym, our method	SymD
1	0.9010	0.9274	0.9254	0.9183	0.9422	**0.9465**	0.9359
2	0.9061	0.9289	0.9281	0.9195	0.9441	**0.9483**	0.9369
3	0.9134	0.9346	0.9345	0.9257	0.9474	**0.9527**	0.9426
4	0.9057	0.9270	0.9261	0.9194	0.9440	**0.9468**	0.9350
5	0.9038	0.9261	0.9258	0.9196	0.9427	**0.9466**	0.9357
6	0.9104	0.9318	0.9312	0.9206	0.9470	**0.9504**	0.9401
7	0.9058	0.9283	0.9270	0.9185	0.9443	**0.9484**	0.9366
8	0.8923	0.9197	0.9191	0.9132	0.9402	**0.9472**	0.9335
9	0.8833	0.9085	0.9091	0.9056	0.9300	**0.9376**	0.9202
10	0.8997	0.9229	0.9225	0.9174	0.9427	**0.9483**	0.9346
11	0.9065	0.9280	0.9253	0.9147	0.9426	**0.9462**	0.9357
12	0.9114	0.9329	0.9325	0.9246	0.9487	**0.9527**	0.9427
13	0.8928	0.9167	0.9152	0.9065	0.9359	**0.9412**	0.9268
14	0.9057	0.9318	0.9305	0.9192	0.9447	**0.9488**	0.9393
15	0.8967	0.9232	0.9219	0.9101	0.9380	**0.9412**	0.9315
16	0.9111	0.9329	0.9314	0.9202	0.9468	**0.9506**	0.9397
17	0.9096	0.9335	0.9315	0.9228	0.9479	**0.9507**	0.9401
18	0.9084	0.9334	0.9326	0.9216	0.9465	**0.9503**	0.9410
19	0.9125	0.9301	0.9274	0.9215	0.9461	**0.9491**	0.9384

from 0 to 1 with higher values indicating better alignment. (3) Dice score (DS) is based on the proportions of tissue overlaps of GM, WM, and CSF. Given two segmentations A and B, the DS is calculated as (Vercauteren *et al* 2009):

$$\mathrm{DS} = \frac{2|A \cap B|}{|A| + |B|} \tag{18}$$

where A and B denote the regions of a specific type of tissues in fixed image and deformed image, respectively. DS can be viewed as a measure of overlap between the two segmentations.

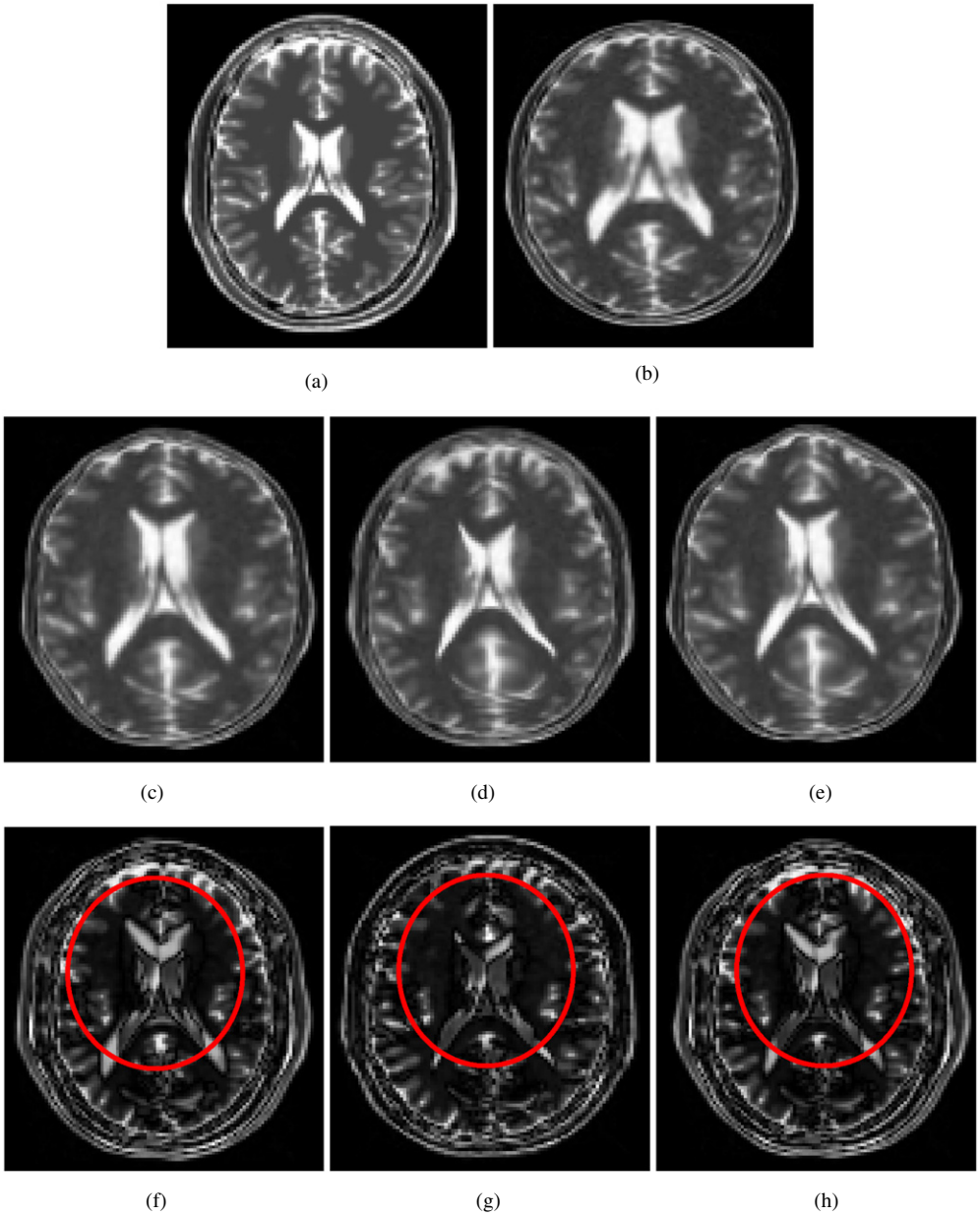

Figure 5. Axial slice of registration results of simulated T2-MRI images using the different algorithms based on symmetric demons forces for (a) a fixed image. (b) a moving image after spherical transformed, (c) a deformed image using DD, (d) a deformed image using our method, (e) a deformed image using SymD, (f) the absolute value of difference in intensity between a deformed image using DD and a fixed image, (g) the absolute value of difference in intensity between a deformed image using our method and a fixed image, (h) the absolute value of difference in intensity between a deformed image using SymD and a fixed image. Regions with most significant differences are highlighted with red circles.

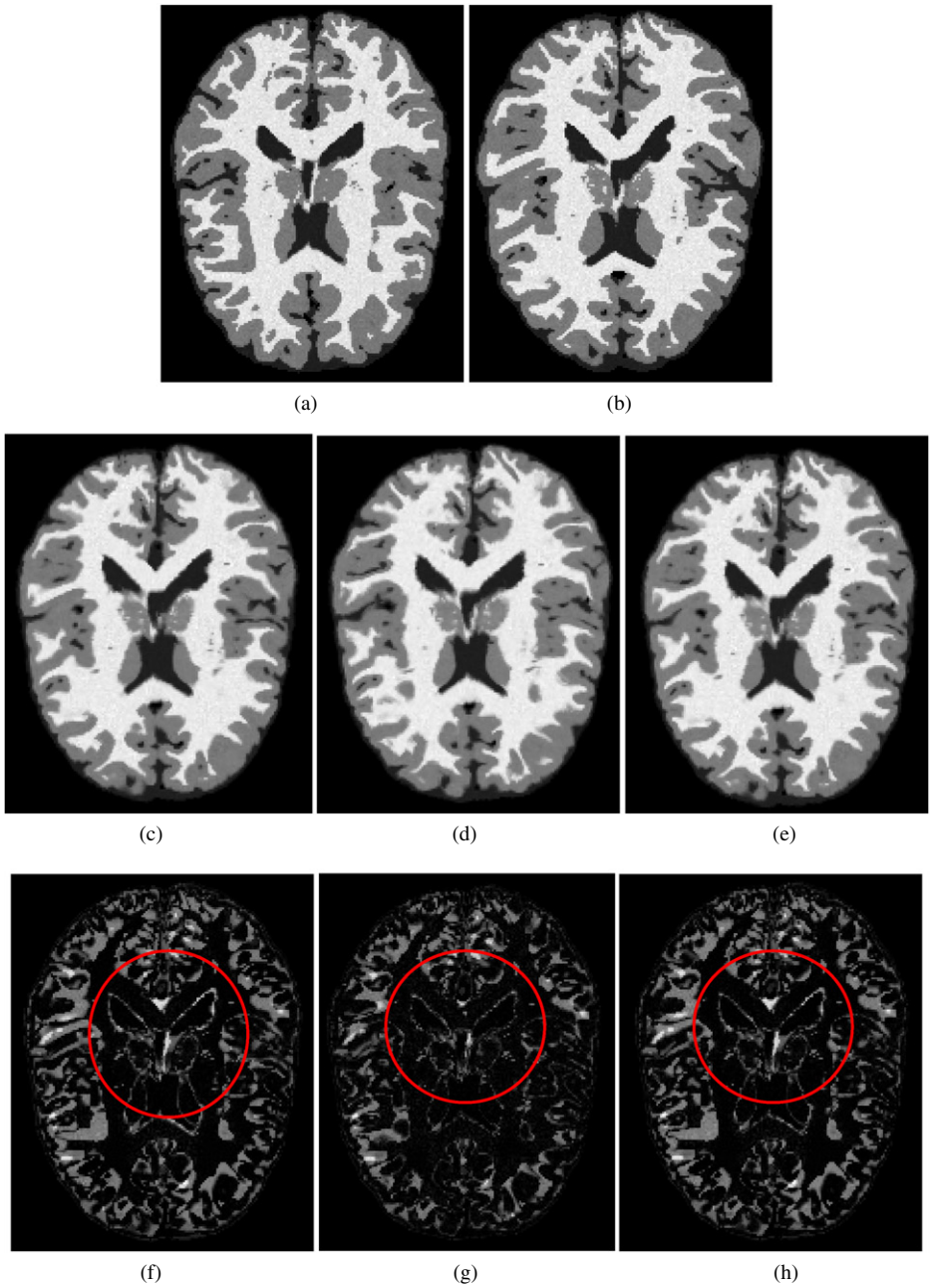

Figure 6. Examples of axial slices of registration results of simulated T1-MRI images using the different algorithms based on symmetric demons forces for (a) a fixed image. (b) a moving image, (c) a deformed image using DD, (d) a deformed image using our method, (e) a deformed image using SymD, (f) the absolute value of difference in intensity between a deformed image using DD and a fixed image, (g) the absolute value of difference in intensity between a deformed image using our method and a fixed image, (h) the absolute value of difference in intensity between a deformed image using SymD and a fixed image,. Regions with most significant differences are highlighted with red circles.

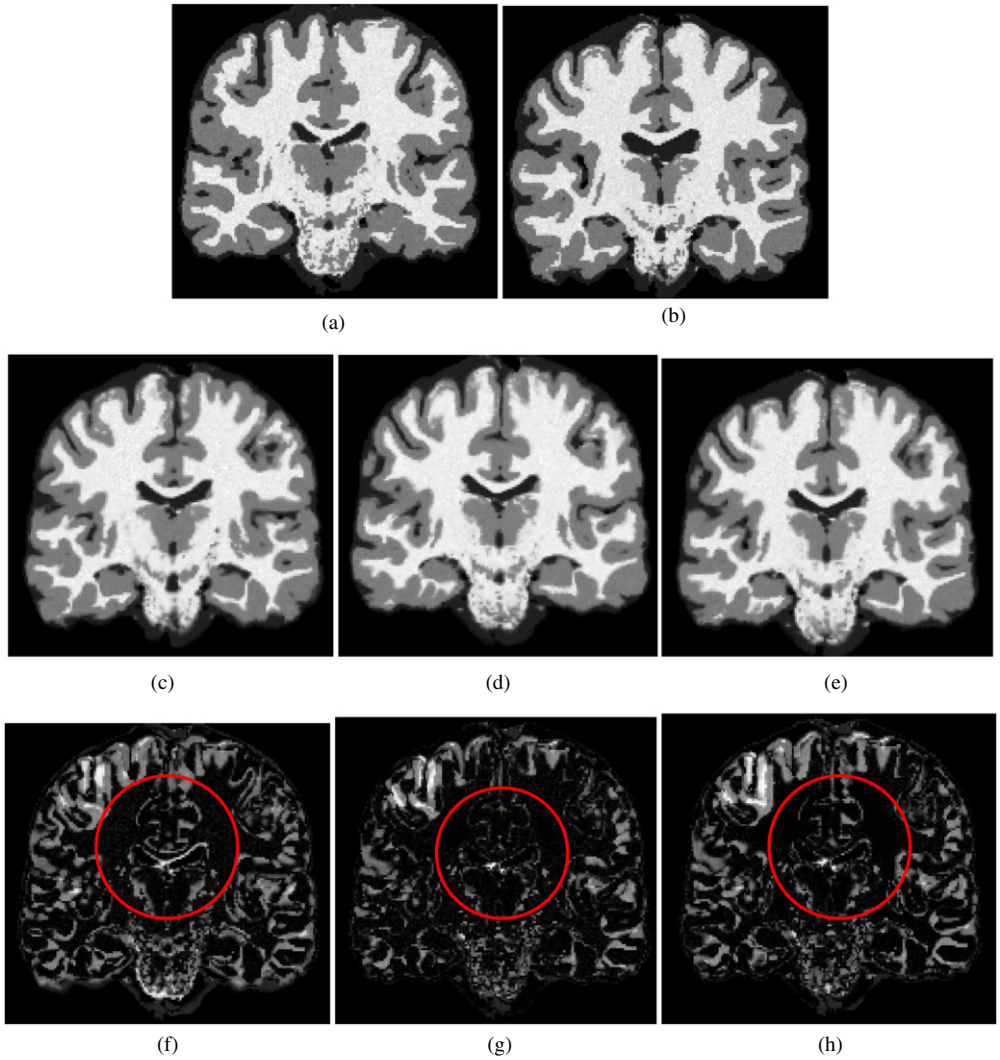

Figure 7. Examples of coronal slices of registration results of simulated T1-MRI images using the different algorithms based on symmetric demons forces for (a) a fixed image. (b) a moving image, (c) a deformed image using DD, (d) a deformed image using our method, (e) a deformed image using SymD, (f) the absolute value of difference in intensity between a deformed image using DD and a fixed image, (g) the absolute value of difference in intensity between a deformed image using our method and a fixed image, (h) the absolute value of difference in intensity between a deformed image using SymD and a fixed image,. Regions with most significant differences are highlighted with red circles.

The more the tissues overlap between the fixed image and the deformed image, the better the registration accuracy. If A and B completely overlap, the DS is equal to 1. If there is no overlap, then the DS is equal to 0.

In our method, we computed image gradients using finite differences. For the parameters of the DD algorithm, optimal values were evaluated in previous work (Rui *et al* 2008): $\sigma_x = 0.5$, the sigma of the Gaussian fluid-like regularization, $\sigma_{\text{flu}} = 1$ and the sigma of

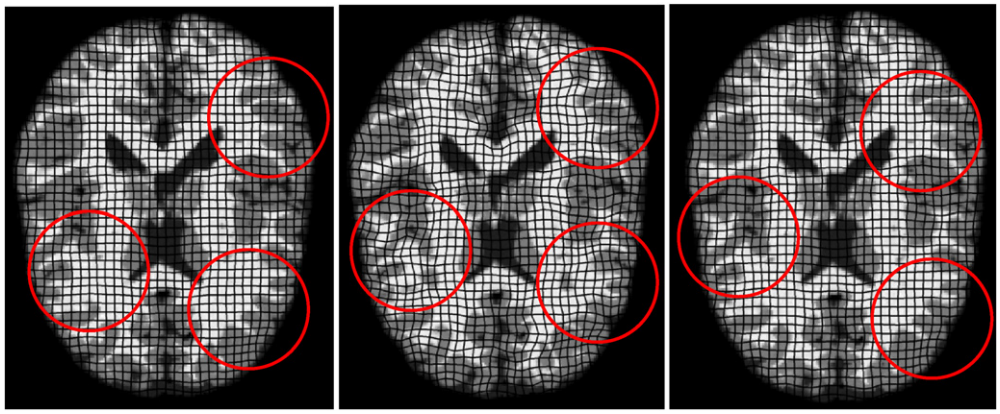

(a) (b) (c)

Figure 8. Deformation field overlapped on the deformed images. (a) Deformation field using DD. (b) Deformation field using our method. (b) Deformation field using SymD. The deformed images (a), (b) and (c) corresponding to the images in figures 6(c)–(e), respectively. Regions with most significant differences are highlighted with red circles.

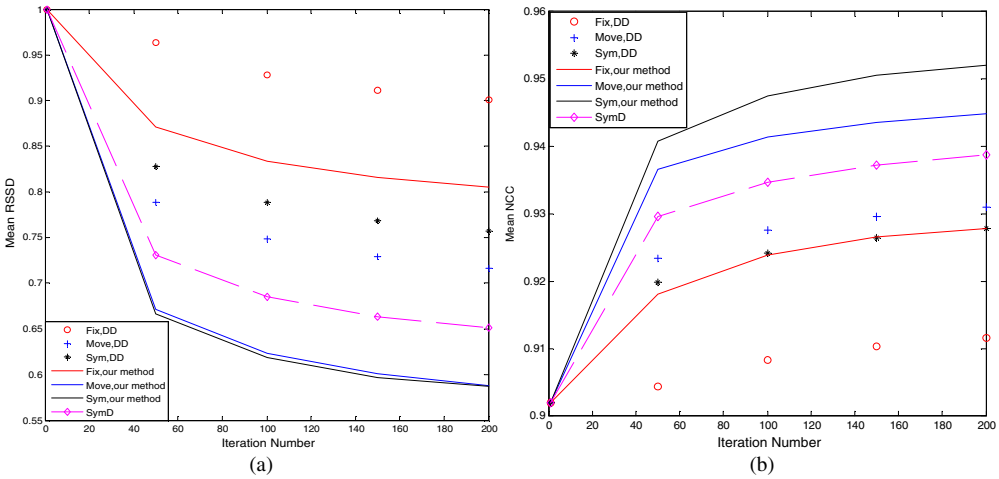

(a) (b)

Figure 9. Performance comparisons of real T1-MRI images by DD, SymD and our method using (a) mean RSSD and (b) mean NCC.

the Gaussian diffusion-like regularization, $\sigma_{\text{diff}} = 1$. For our method, we empirically set σ_y equal to $3^*\sigma_x$. In addition, a maximum of 200 iterations was used to ensure convergence for all methods. In the first experiment, the MRI images with 0% noise level and 0% intensity non-uniformity were selected as templates and the remaining datasets were wrapped around a 3D concentric sphere (Pratt 2002) to obtain the moving images, respectively. Then we registered these moving images to their corresponding template using the different methods. The mean RSSD and NCC over the registered images were inspected. In the second and third experiments, one of the images was randomly selected as a template and the remaining datasets were all registered to this template using the various methods. The mean RSSD, NCC and DS over the registered MRI images were examined and compared.

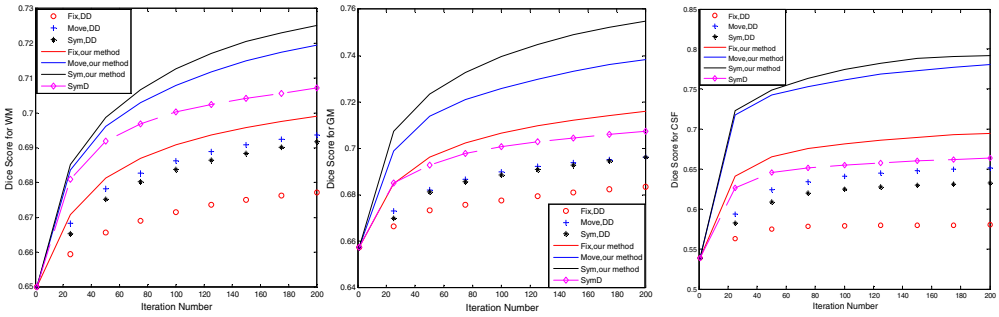

(a) (b) (c)

Figure 10. Comparisons of Dice Scores for the three tissue types of the real T1-MRI images: white matter, grey matter and cerebrospinal fluid. (a) Dice score for white matter. (b) Dice score for gray matter. (c) Dice score for CSF.

Table 3. Comparisons of the normalized cross correlation obtained from the registration of the real T1-weighted MR images. The column is number of the sample data. The row is the results of different methods. The best results are shown in bold.

	Fix, DD	Move, DD	Sym, DD	Fix, our method	Move, our method	Sym, our method	SymD
1	0.9319	0.9548	0.9465	0.9443	**0.9800**	0.9798	0.9583
2	0.9254	0.9509	0.9458	0.9442	**0.9659**	0.9634	0.9567
3	0.9323	0.9608	0.9565	0.9535	**0.9750**	0.9736	0.9637
4	0.9488	0.9685	0.9638	0.9588	**0.9805**	0.9803	0.9683
5	0.9219	0.9428	0.9350	0.9362	0.9715	**0.9763**	0.9493
6	0.8703	0.8879	0.8847	0.8951	0.8982	**0.9145**	0.9028
7	0.8827	0.8995	0.8965	0.9033	0.9082	**0.9217**	0.9176
8	0.9219	0.9450	0.9408	0.9352	**0.9557**	0.9537	0.9479
9	0.8838	0.8996	0.8976	0.9002	0.9094	**0.9195**	0.9139
10	0.9184	0.8960	0.9125	0.9331	0.8549	**0.9087**	0.9053
11	0.8994	0.9160	0.9137	0.9125	0.9259	**0.9305**	0.9267
12	0.9376	0.9622	0.9585	0.9530	**0.9745**	0.9730	0.9635
13	0.9169	0.9500	0.9446	0.9402	**0.9738**	0.9732	0.9536
14	0.8706	0.8997	0.8936	0.8809	0.9536	**0.9607**	0.9149
15	0.8869	0.8850	0.8874	0.9067	0.8951	**0.9096**	0.9071
16	0.9222	0.9327	0.9294	0.9356	**0.9455**	0.9427	0.9386
17	0.8943	0.8981	0.8983	0.9079	0.9089	**0.9139**	0.9083

3.2. Experimental results

3.2.1. Simulated images experiments. In the first experiment, the NCC and RSSD curves changed rapidly before 40 iterations and became relatively stable afterwards (figure 2). Over a range of iterations, the performance of our method using different demons forces were superior to those of DD and SymD in terms of mean RSSD (figure 2(a)). The RSSD comparison indicated that our method can provide a good trade-off between degree of matching intensity and the degree of deformation in the registration process. Our method also performed better in terms of mean NCC, which indicted using our methods resulted in a better global alignment than did the DD algorithms (figure 2(b)). Therefore, our method outperformed the DD and SymD methods in term of mean NCC and mean RSSD in registration of T2-weighted images

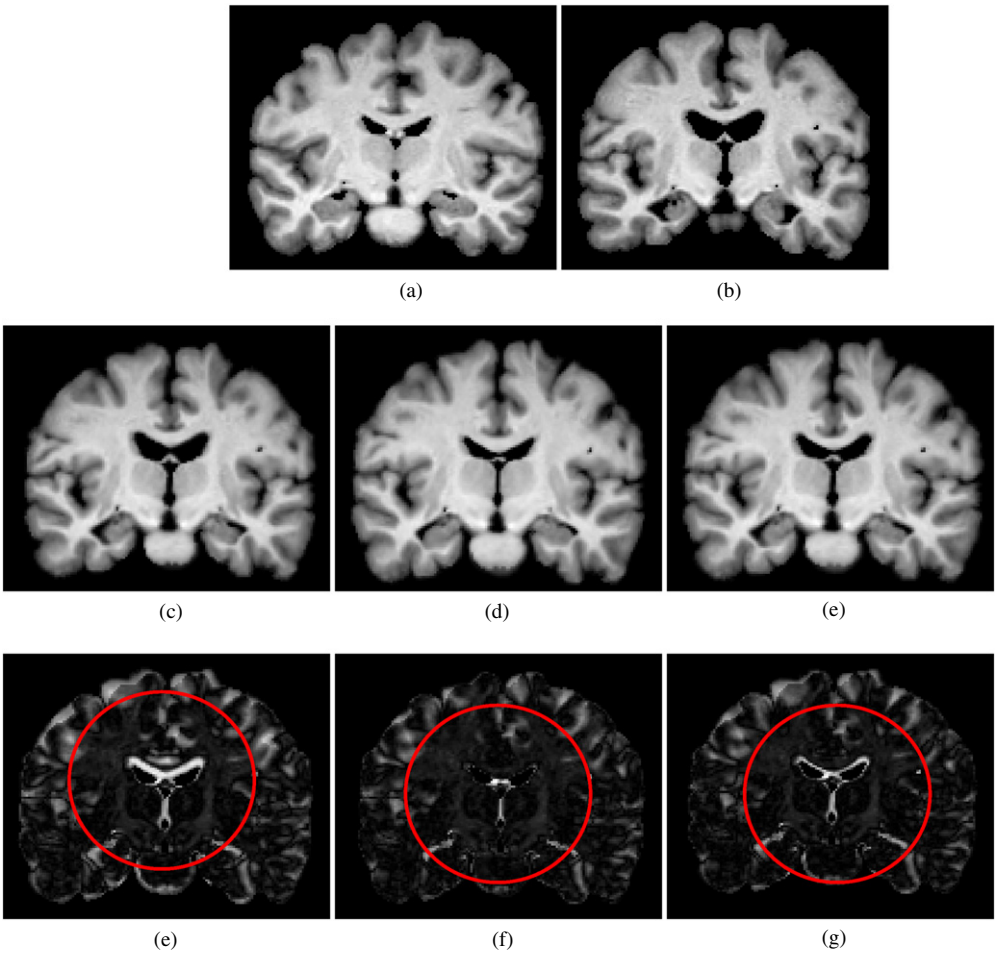

Figure 11. Examples of coronal slices of registration results of real T1-MRI images using the different algorithms based on symmetric demons forces for (a) a fixed image. (b) a moving image, (c) a deformed image using DD, (d) a deformed image using our method, (e) a deformed image using SymD, (f) the absolute value of difference in intensity between a deformed image using DD and a fixed image, (g) the absolute value of difference in intensity between a deformed image using our method and a fixed image, (h) the absolute value of difference in intensity between a deformed image using SymD and a fixed image,. Regions with most significant differences are highlighted with red circles.

at differing noise and intensity non-uniformity levels (figure 2), which demonstrated that our method is robust in registering medical images.

In the second experiments, the convergence properties of the registration methods were similar to those in the first experiments (figures 3 and 4). The mean RSSD and NCC comparisons were also similar to those in the first experiments. Meanwhile, in term of mean DS our method using a fixed image force outperformed the different variants of DD. For DD, the SymD force and moving image force obtained similar registration results (figures 3 and 4). The mean DS of our method offered about 10% improvement over the mean DS of the DD algorithms. For all these methods, the moving force obtained better results than did the fixed

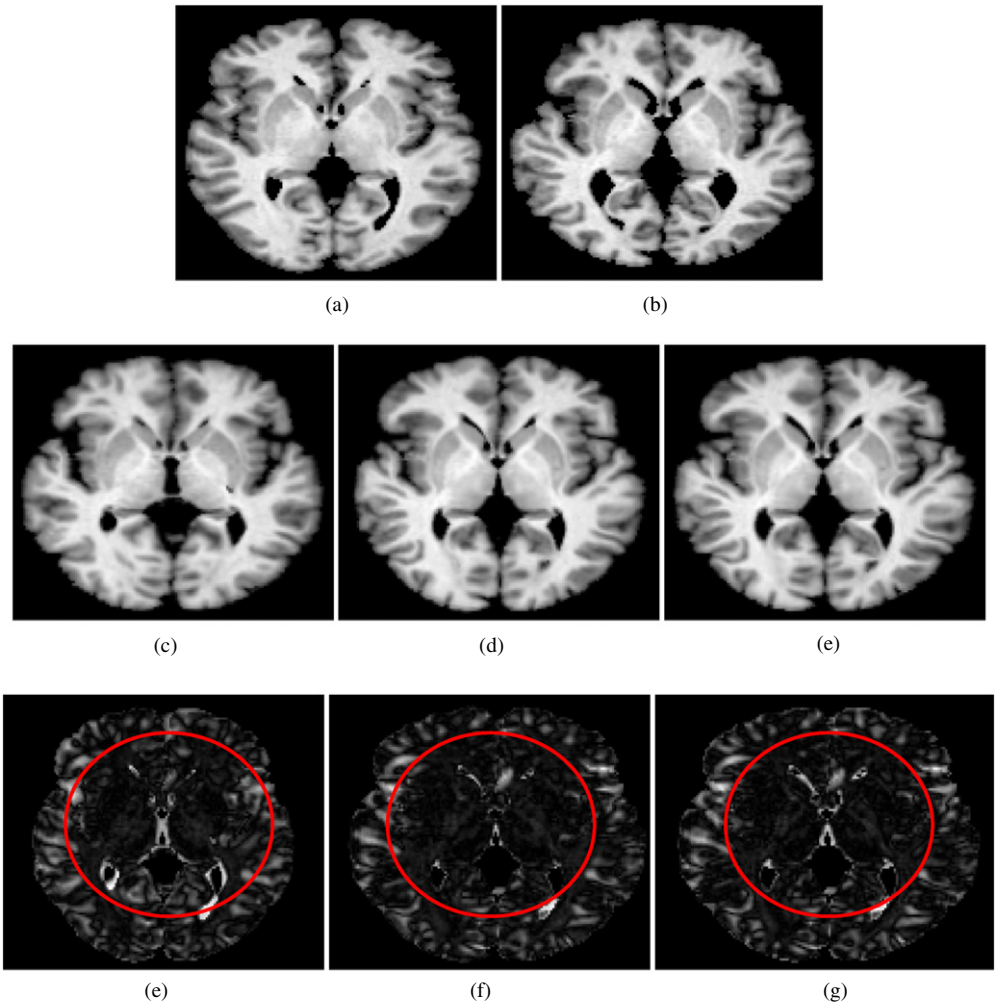

Figure 12. Examples of coronal slices of registration results of real T1-MRI images using the different algorithms based on symmetric demons forces for (a) a fixed image. (b) a moving image, (c) a deformed image using DD, (d) a deformed image using our method, (e) a deformed image using SymD, (f) the absolute value of difference in intensity between a deformed image using DD and a fixed image, (g) the absolute value of difference in intensity between a deformed image using our method and a fixed image, (h) the absolute value of difference in intensity between a deformed image using SymD and a fixed image. Regions with most significant differences are highlighted with red circles.

image force. For the overall performance in term of NCC (table 2), the symmetric force of our method also achieved the best results in almost all the cases of the sample data.

To visualize the registration accuracy of the proposed method, we showed the registered MRI images of various methods with symmetric demons forces (figures 5, 6 and 7). Our method visually outperformed the DD and SymD methods as mirrored by the more accurate boundary information of the registered MRI images, which are benefitted by structural information (gradient magnitude) matching. The residual images of our method also showed lower values than that of DD and SymD (figures 5(f)–(h), 6(f)–(h), 7(f)–(h)).

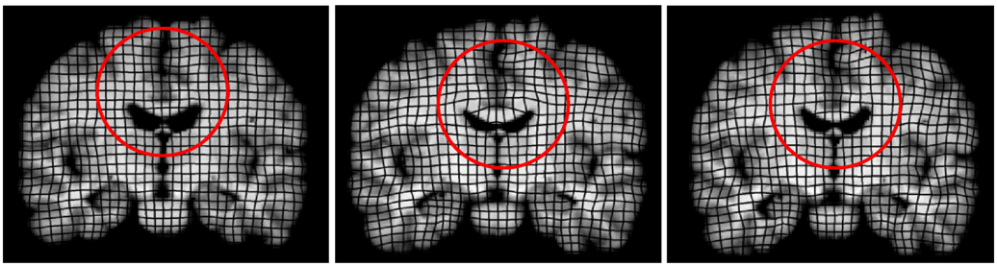

(a) (b) (c)

Figure 13. Deformation field overlapped on the deformed images. (a) Deformation field using DD. (b) Deformation field using our method. (b) Deformation field using SymD. The deformed images (a), (b) and (c) corresponding to the images in figures 11(c)–(e), respectively. Regions with most significant differences are highlighted with red circles.

Although the deformed images did not match the fixed image entirely (figures 6(a) and 7(a)), the deformation fields of DD and SymD were too smooth to model further deformations (figures 8(a) and (c)). The deformation field of our method was more capable of modeling large deformations, which benefitted from structure information (gradient magnitude) matching (figure 8(b)).

3.2.2. Real image experiments. For real MRI images, the experiments were set up like that for the simulated MRI data. The registration results were consistent with those of the experiments using simulated MRI data. The results of RSSD and mean NCC were similar with the ones presented in the simulated image experiments (figures 2 and 3). Our methods with moving force and symmetric force performed better than the DD and SymD with different demons forces (figure 9). The moving force of both methods obtained the best results than did the other demons forces in this experiment. For DS comparisons, the results are similar to the ones presented in figure 4. Again, our method with the moving force and symmetric force also performed better than the different variants of DD and SymD (figure 10). It is shown that the proposed method maintains a higher registration accuracy than DD and SymD. For the overall performance in term of NCC (table 3), the moving force and symmetric force of our method achieved the best results in almost all cases of all the sample data.

Visual assessment shows that the proposed method outperformed DD and SymD as mirrored by the more accurate structural information of the registered images, which matched the findings obtained in the experiments of the simulated MRI image (figures 11 and 12). Especially in the ventricular region, the results of our method obtained a much better alignment than did those of DD and SymD (figures 11(c) and (e); figures 12(c) and (e)). The deformation field of our method is also better at modeling further deformation information than those of DD and SymD (figure (13)).

4. Conclusion and discussion

To improve the accuracy and efficiency of anatomical alignment in medical image registration, we proposed a new dissimilarity measure for demons-type algorithms by combining the differences of both image intensity and gradient magnitude. By optimizing the new dissimilarity criteria, we developed a chain-type DD algorithm. We also provided different demons forces of the new method, which included both the gradient of the image gradient

and gradient magnitude. We tested the effectiveness of our method on both T1-weighted and T2-weighted images and also compared our method with two most popular demons-type algorithms, i.e., the DD and SymD algorithms. In the experiments, we examined these methods based on the mean results of RSSD, NCC and DS across all the sample data, and also conducted overall comparisons in term of NCC (tables 2 and 3). These results were consistent on both simulated and real MRI datasets, which demonstrated that our method was the most effective and robust in registering medical images.

In the first experiment, we evaluated the robustness of the registration algorithms using the deformed moving images at differing noise and intensity non-uniformity levels. Noted that the major difference between our method and the DD and SymD methods is that our method uses a new dissimilarity measure that jointly considers the differences of both image intensity and gradient magnitude for the demons algorithm. While the DD and SymD algorithms use only the difference of image intensity for the demons algorithm. The improvement of the registration results demonstrated that the new dissimilarity measure is effective for the registration of medical images when noise and intensity non-uniformity present.

Our experiments were performed based on MATLAB R2010a. Neither specially precompiled routines nor look-up tables were used to accelerate the computation. For the real MRI data from IBSR, we found that the computation time per iteration was approximately 29.08 s for DD using the symmetric force, 35.34 s for SymD and 38.30 s for our method using the same symmetric force. The major different between our method and the DD method is the computation of the gradient in the gradient images. However, the DD algorithms were implemented using a C++ based on the ITK library (www.itk.org) which was reported in previous works (Vercauteren *et al* 2008). With a difference computational cost of only about 6 to 9 s and knowing Matlab has been complained for years for its low computational performance, we are confident that our algorithm will perform much more efficient than does the DD algorithm if they can be compared on the same platform which forms a fairly basis for the comparison. Therefore, we think that our method may be a better alternative for real-life applications.

Similar to our method, a multi-channel registration method is popular, which combines different image features to improve registration accuracy (Daniel *et al* 2011, Jean-Marc *et al* 2010, Park *et al* 2003). However, our method unifies different features into one deformation field, while a multi-channel method obtains multiple deformation fields and then fuses them by an additive rule. The additive rule used in multi-channel method makes the registration process not diffeomorphic, while the chain-type DD method can use multiple channel information and remain diffeomorphic altogether.

In our method, we used gradient magnitude images to represent structural information of an image and utilized the difference in gradient magnitude to improve registration accuracy. We employed the simplest numerical gradient in our method for its easy understanding and simple calculation. Actually, many local-type information of an image have been developed and have achieved good performance in image processing (Cheng and Mrinal 2010, Roger *et al* 2003). However, comparing these local-type information of an image in medical image registration is not the focus of our study, we just placed the algorithm framework of the new method here.

Researchers have proposed many excellent non-rigid registration methods, and the DD algorithm and SymD algorithm are two popular ones among them in recent years. Detailed comparisons of these registration methods have been done in many works (Hernandez *et al* 2008, Klein *et al* 2009). In this paper, we made a comprehensive comparison between our method and these two algorithms. Further comparisons with other registration methods will be done in future work.

Acknowledgment

This work was supported by the Zhejiang Provincial Natural Science Foundation of China (grant no. LZ12F02004).

References

Arsigny V, Commonwick O, Pennec X and Ayache N A log–Euclidean framework for statistics on diffeomorphisms *Medical Image Computing and Computer Assisted Intervention—MICCAI 2006* (*Lecture Notes in Computer Science* vol 4190) (Heidelberg: Springer) pp 924–31

Ashburner J 2007 A fast diffeomorphic image registration algorithm *NeuroImage* **38** 95–113

Avants B, Grossman M and Gee J 2006 Symmetric diffeomorphic image registration: Evaluating labeling of elderly and neurodegenerative cortex and frontal lobe *Biomedical Image Registration* (*Lecture Notes in Computer Science* vol 4057) ed J PW Pluim, B Likar and F A Gerritsen (Heidelberg: Springer) pp 50–57

Beg M F, Miller M I, Trouv′e A and Younes L 2005 Computing large deformation metric mappings via geodesic flows of diffeomorphisms *Int. J. Comput. Vis.* **61** 113–34

Cachier P, Bardinet E, Dormont D, Pennec X and Ayache N 2003 Iconic feature based nonrigid registration: the PASHA algorithm *Comput. Vis. Image Underst.* **89** 272–98

Cheng L and Mrinal M 2010 Improved demons technique with orthogonal gradient information for medical image registration *IEICE Trans. Inf. Syst.* **E93.D** 3414–7

Daniel J *et al* 2011 Patient specific dosimetry phantoms using multichannel LDDMM of the whole body *Int. J. Biomed. Imaging* **2011** 481064

Gu X *et al* 2010 Implementation and evaluation of various demons deformable image registration algorithms on a GPU *Phys. Med. Biol.* **55** 207–19

Hawkes D J 1999 Nonrigid registration using free-form deformations: application to breast MR images *IEEE Trans. Med. Imaging* **18** 712–21

Hernandez M and Olmos S 2008 Gauss–Newton optimization in diffeomorphic registration *ISBI'08: 5th IEEE Int. Symp. on Biomedical Imaging: From Nano to Macro* pp 1083–6

Hernandez M, Olmos S and Pennec X 2008 Comparing algorithms for diffeomorphic registration: stationary LDDMM and diffeomorphic demons *Proc. 2nd MICCAI workshop on Mathematical Foundations of Computational Anatomy* pp 24–35

Holden M 2008 A review of geometric transformations for nonrigid body registration *IEEE Trans. Med. Imaging* **27** 111–28

Jean-Marc P, Herve D, Maxime S, Chenyang X and Nicholas A 2010 Registration of 4D cardiac CT sequences under trajectory constraints with multichannel diffeomorphic demons *IEEE Trans. Med. Imaging* **29** 1351–68

Kai B and Uwe D H 2001 Template matching using fast normalized cross correlation *Proc. SPIE* **4387** 4387–95

Klein A *et al* 2009 Evaluation of 14 nonlinear deformation algorithms applied to human brain MRI registration *Neuroimage* **46** 786–802

Kroon D J and Slump C H 2009 MRI modality transformation in demon registration *ISBI'09: IEEE Int. Symp. on Biomedical Imaging: From Nano to Macro* pp 963–6

Luo Y and Chung A C 2009 Non-rigid image registration using local histogram-based features *EMBS'09: Proc. IEEE Conf. Engineering in Medicine and Biological Society* vol 2009 pp 5793–6

Modat M, Vercauteren T, Ridgway G R, Hawkes D J, Fox N C and Ourselin S 2010 Diffeomorphic demons using normalized mutual information, evaluation on multimodal brain MR images *Proc. SPIE* **7623** 76232K

Nathan D C, Noble J A and David J H 2009 A demons algorithm for image registration with locally adaptive regularization *Med. Image Comput. Comput. Assist. Intervention—MICCAI 2006 (Lecture Notes in Computer Science* vol 5761*)* (Heidelberg: Springer) pp 574–81

Park H J *et al* 2003 Spatial normalization of diffusion tensor MRI using multiple channels *NeuroImage* **20** 1995–2009

Pennec X, Cachier P and Ayache N 1999 Understanding the demons algorithm: non-rigid registration by gradient descent *Medical Image Computing and Computer Assisted Intervention—MICCAI 1999* (*Lecture Notes in Computer Science* vol 1679) (Heidelberg: Springer) pp 597–605

Pratt W K 2002 *Digital Image Processing: PIKS Inside* 3rd edn (New York: Wiley)

Rogel J R and Kovacic S 2006 Symmetric image registration *Med. Image Anal.* **10** 484–93

Roger L, Ewert B and Lennart T 2003 A combined intensity and gradient-based similarity criterion for interindividual SPECT brain scan registration *EURASIP J. Adv. Sig. Proc.* **2003** 461–9

Rueckert D, Aljabar P, Heckemann R A, Hajnal J V and Hammers A 2006 Diffeomorphic registration using B-splines *Medical Image Computing and Computer Assisted Intervention—MICCAI 2006* (*Lecture Notes in Computer Science* vol 4191) ed R Larsen, M Nielsen and J Sporring (Heidelberg: Springer) pp 702–9

Rui G, Albert C S and Shu L 2008 Maximum distance-gradient for robust image registration *Med. Image Anal.* **12** 452–68

Sabuncu M, Yeo B, Vercauteren T, Leemput K V and Golland P 2009 Asymmetric image template registration *Medical Image Computing and Computer Assisted Intervention—MICCAI 2009 Part I* (*Lecture Notes in Computer Science* vol 5761) ed G-Z Yang *et al* (Heidelberg: Springer) pp 565–73

Thirion J P 1998 Image matching as a diffusion process: an analogy with Maxwell's demons *Med. Image Anal.* **2** 243–60

Vercauteren T, Pennec X, Perchant A and Ayache N 2008 Symmetric log-domain diffeomorphic registration: a demons-based approach *Medical Image Computing and Computer Assisted Intervention—MICCAI 2008:Part I* (*Lecture Notes in Computer Science* vol 5241) ed D Metaxas, L Axel, G Fichtinger and G Sz′ekely (Heidelberg: Springer) pp 754–61

Vercauteren T, Pennec X, Perchant A and Ayache N 2009 Diffeomorphic demons: efficient non-parametric image registration *NeuroImage* **45** 61–72

Wang H *et al* 2005 Validation of an accelerated 'demons' algorithm for deformable image registration in radiation therapy *Phys. Med. Biol.* **50** 2887–905